# 细丝大电流 MAG 焊的熔滴过渡机制

华爱兵[1]， 殷树言[2]， 陈树君[2]， 白韶军[2]， 张晓亮[2]
（1. 北京中电华强焊接工程技术有限公司，北京 100076；
2. 北京工业大学 机械工程及应用电子技术学院，北京 100124）

摘 要：借助高速摄像分析了两种常规混合气体（80%Ar+20%$CO_2$ 和 98%Ar+2%$O_2$）保护的细丝大电流 MAG 焊的基本特点，研究了焊丝伸出长度和保护气体成分对第二临界电流的影响规律，揭示了细丝大电流 MAG 焊的熔滴过渡机制．同时详细地分析了离心破断过渡、混合过渡和旋转短路过渡的产生条件和形成过程．并指出了 80%Ar+20%$CO_2$ 气体保护的细丝大电流 MAG 焊之所以无法应用的根本所在，从而确立了 98%Ar+2%$O_2$ 气体保护的细丝大电流 MAG 焊实现高效化焊接的可行性．

关键词：细丝大电流活性气体保护焊；第二临界电流；离心破断过渡；旋转短路过渡
中图分类号：TG115.28 文献标识码：A 文章编号：0253－360X(2009)08－0093－04

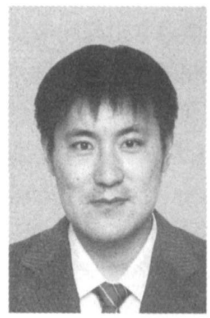

华爱兵

## 0 序 言

当采用较细直径的焊丝（一般不大于 $\phi$1.2 mm），若焊接电流超过第二临界电流，同时配合较大的焊丝伸出长度（通常都大于 15 mm）和较高的电弧电压，电弧将偏离焊丝轴线一定角度并绕焊丝轴线高速旋转，形成所谓的“旋转射流过渡”．将具有这些特点的 MAG 焊称为细丝大电流 MAG 焊，它通常应用于平板堆焊、角焊缝等场合[1－3]．

目前较为成功的细丝大电流 MAG 焊当属 T.I.M.E.焊[4,5]，它采用特殊的四元混合保护气体（0.5%$O_2$，8%$CO_2$，26.5%He，65%Ar），通过增大送丝速度将焊丝熔敷率提高了 2～3 倍．但是从掌握的资料看，Fronius 公司除了简单提供 T.I.M.E.焊的基本特点和适用范围外，并没有在焊接机理方面作进一步的介绍，因此这方面的资料相当匮乏．同时由于 T.I.M.E.焊的保护气体中含有较多的氦，并且气体配比要求高，再加上使用过程中存在知识产权等问题，制约了该工艺在国内的推广应用[6]．

鉴于此，文中借助高速摄像分析了两种常规无氦混合气体保护的细丝大电流 MAG 焊的基本特点，揭示了这种高效 MAG 焊接工艺的熔滴过渡机制，并澄清了人们在该领域的一些模糊认识，从而为实现常规无氦混合气体保护的细丝大电流 MAG 焊的工程应用提供了理论依据和技术支持．

## 1 细丝大电流MAG 焊的第二临界电流

通过大量的试验发现，细丝大电流 MAG 焊的第二临界电流值 $I_{lj}$与焊丝伸出长度 $L_e$ 和保护气体成分密切相关，这一关系如图 1 所示．

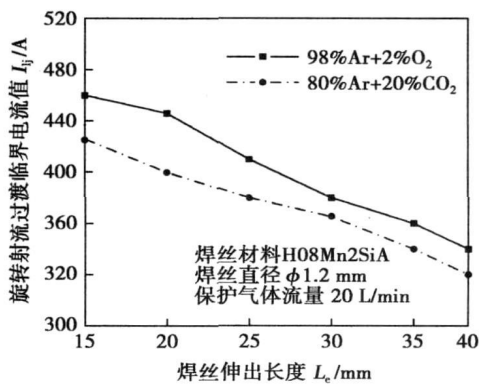


图 1 细丝大电流 MAG 焊的第二临界电流值

Fig. 1 The second critical current of MAG welding with high-current density

由图 1 可知，随着焊丝伸出长度 $L_e$ 的提高，细丝大电流 MAG 焊的第二临界电流值都下降；然而当焊丝伸出长度 $L_e$ 相同时，保护气体为 98%Ar+2%

收稿日期：2008－06－12

$O_2$ 的第二临界电流值要比保护气体为 80%Ar+20%$CO_2$ 的大一些.

## 2 细丝大电流MAG 焊的熔滴过渡机制

根据焊接工艺参数和保护气体成分的不同, 细丝大电流MAG 焊的熔滴过渡方式大体上分为三种, 离心破断过渡、混合过渡和旋转短路过渡, 其中离心破断过渡通常出现在 98%Ar+2%$O_2$ 气体保护且电弧电压相对较高的情况; 而混合过渡方式(即离心破断过渡和电爆炸过渡相结合)往往发生在 80%Ar+20%$CO_2$ 气体保护且电弧电压较高的时候; 无论采用 98%Ar+2%$O_2$ 或者 80%Ar+20%$CO_2$, 当送丝速度过快或者电弧电压过低, 电弧长度急剧减小, 甚至液流束与熔池瞬时接触, 这时细丝大电流 MAG 焊容易产生旋转短路过渡.

### 2.1 离心破断过渡

图 2 给出了 98%Ar+2%$O_2$ 气体保护时细丝大电流MAG 焊接过程的一组高速摄像片断, 试验所采用的参数为: 送丝速度为 27 m/min, 焊接电流为 515 A 左右, 电弧电压为 53 V; 焊丝材料为 H08Mn2SiA, 焊丝直径为 1.2 mm, 焊丝伸出长度 25 mm; 保护气体流量为 25 L/min, ; 工件采用 Q235, 其厚度为 10 mm; 焊接速度为 0.7 m/min; 高速摄像机的拍摄速度为 3 000 祯/s, 拍摄方向与焊接方向相垂直.

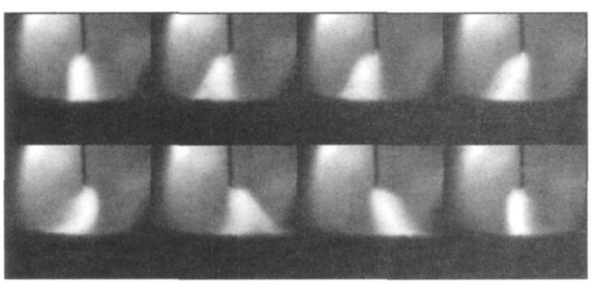

图 2 98% Ar+2% $O_2$ 气体保护的细丝大电流 MAG 焊

Fig. 2 High current density MAG welding process with 98% Ar+2% $O_2$

从图 2 中可以看出 98%Ar+2%$O_2$ 气体保护的细丝大电流MAG 焊的基本特点[2].

(1) 电弧形态呈钟罩状, 焊丝端部的液态金属呈细锥状(称之为"液锥"), 而液锥下端悬挂一条流束形的黑线(称之为"液流束").

(2) 电弧、液锥和液流束都偏离了焊丝轴线并绕焊丝轴线高速旋转.

(3) 电弧烁亮区均匀包覆了大部分液锥和全部的液流束.

(4) 熔滴过渡轨迹虽然偏离了焊丝轴线, 但是始终在电弧烁亮区内进行, 焊接过程稳定, 基本无飞溅.

图 3 给出了这种稳定的细丝大电流MAG 焊的熔滴过渡过程示意图, 它大致可以分为四个阶段: 液流束形成(图 3a)、液流束长大(图 3b)、液流束与液锥分离的同时破断成大量的金属小液滴(图 3c)、金属小液滴在自身惯性的作用下沿各个方向向焊接熔池过渡, 并且液锥末端形成新的液流束(图 3d), 随后新的液流束将再次长大、破断, 并重复上述焊接过程.

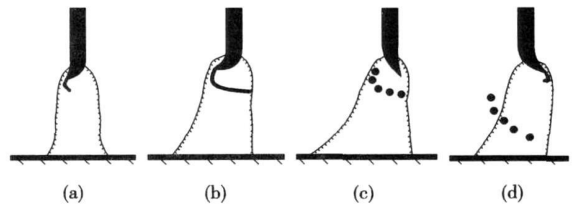


图 3 稳定细丝大电流 MAG 焊的熔滴过渡过程

Fig. 3 Droplet transfer process of steady MAG welding with high-current density

长期以来, 焊接工作者总是习惯性地称上述过渡方式为"旋转射流过渡", 然而"旋转射流过渡"并不能反映这种过渡方式的本质特征. 所谓"射流"就意味着强等离子流的存在, 并且在该强等离子流的作用下, 细小的熔滴从焊丝端头沿焊丝轴线以较高的速度射出. 而 98%Ar+2%$O_2$ 气体保护的细丝大电流MAG 焊电弧偏离焊丝轴线较大的角度并且绕焊丝轴线高速旋转, 显然不能形成强等离子流. 另外从高速摄像结果看, 液流束向熔池过渡时虽然在电弧烁亮区内部进行, 但是并没有沿着焊丝轴线.

既然强等离子流不存在, 那么促进熔滴过渡的驱动力到底是什么呢?

众所周知, 细丝大电流MAG 焊的典型特征表现为电弧和焊丝端部的液体金属绕焊丝轴线高速旋转, 那么液锥末端的液流束必将受到较强的旋转离心力的作用. 实际上正是由于旋转离心力的存在, 使得液流束能够克服液锥的束缚, 并且当液流束顺畅地脱离液锥后破断成大量的金属小液滴, 然后这些金属小液滴在自身惯性作用下沿各个方向过渡到熔池中去. 可见, 98%Ar+2%$O_2$ 气体保护的细丝大电流 MAG 焊的熔滴过渡方式称为"离心破断过渡"更为确切, 更能反映这种高效焊接工艺的本质特征.

### 2.2 混合过渡

当保护气体采用 80%Ar+20%$CO_2$ 时, 细丝大

电流 MAG 焊接过程如图 4 所示, 试验参数为: $v_f$=25 m/min, $I$=470 A 左右, $U_a$=52 V, $L_e$=20 mm, 保护气体流量为 20 L/min, 其它参数同 2.1 节.

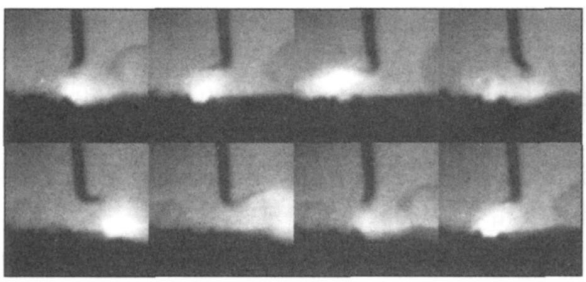

图 4　80%Ar+20%$CO_2$ 气体保护的细丝大电流 MAG 焊

Fig. 4　High-current density MAG welding with 80%Ar+20%$CO_2$

由图 4 可知:

(1) 电弧和焊丝端部的液态金属都偏离了焊丝轴线较大的角度并绕焊丝轴线高速旋转.

(2) 电弧的运动滞后于液锥的运动.

(3) 电弧烁亮区呈球状, 并且电弧烁亮区包覆液锥的面积过少, 基本上仅包覆液锥的尖端, 甚至出现了电弧烁亮区只包覆液锥一侧的现象.

(4) 熔滴过渡方式表现为液流束被快速地横向甩出, 并形成了较大的焊接飞溅.

显然, 80%Ar+20%$CO_2$ 气体保护的细丝大电流MAG 焊是一个不稳定的、无规律的过程, 而图 5 则进一步给出了这种非稳定的细丝大电流 MAG 焊接过程示意图.

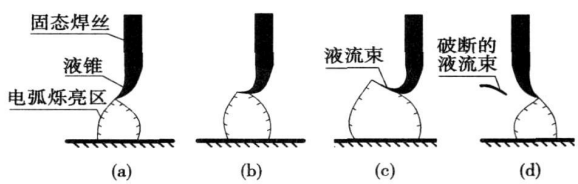


图 5　非稳定的细丝大电流 MAG 焊的熔滴过渡过程

Fig. 5　Droplet transfer process of unsteady MAG welding with high-current density

由于 $CO_2$ 气体高温下分解吸热并压缩电弧, 同时电弧的高速旋转加剧了周围气体对电弧的冷却作用, 其结果导致电弧电场强度较高, 并使得电弧上爬困难, 因此电弧包覆液锥的面积过少, 甚至仅包覆液锥的尖端(图 5a). 显然, 此时电弧将对液锥产生较强的排斥作用, 使得液锥偏角(即液锥偏离焊丝轴线的角度)逐渐变大(图 5b). 在电阻热和电弧热的共同作用下, 液锥下端开始形成细长的液流束, 伴随着液流束长度的增加, 电弧的亮度变暗, 并且电弧包覆着液流束的底部(图 5c). 这时候由于液流束高速旋转所形成的旋转离心力以及焊接电流通过细长的液流束所产生的爆炸力, 容易造成液流束成段飞出(图 5d), 并形成大量的焊接飞溅.

综上所述, 80%Ar+20%$CO_2$ 气体保护的细丝大电流 MAG 焊的液流束是在旋转离心力和爆炸力的共同作用下脱离液锥的束缚, 因此这种过渡方式应该为离心破断过渡和电爆炸过渡的合成, 简称为"混合过渡".

### 2.3　旋转短路过渡

旋转短路过渡通常发生在电弧电压过低或者送丝速度过快的情况, 如图 6 所示. 试验条件为: $v_f$=28 m/min, $I$=500 A 左右, $U_a$=44 V, $L_e$=25 mm, 保护气体采用 80%Ar+20%$CO_2$, 保护气体流量为 25 L/min, 其它参数同 2.1 节.

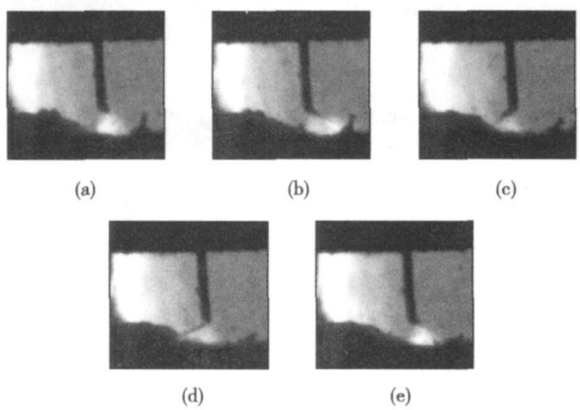


图 6　细丝大电流 MAG 焊的短路现象(80%Ar+20%$CO_2$)

Fig. 6　Shorting transfer process of high-current density MAG welding with 80%Ar+20%$CO_2$

从图 6 中可以看出高速旋转短路过渡 MAG 焊接过程为: 电弧燃烧后, 由电弧析出热量, 熔化焊丝, 并且在固态焊丝端头形成液锥(图 6a). 随后液锥的末端开始形成了一条细长的液流束, 同时电弧长度减小(图 6b). 随着液流束长度的不断加大, 电弧向未熔化焊丝方向传入的热量减少, 则焊丝的熔化速度降低. 由于焊丝仍保证以一定速度送进, 势必增大了液流束与熔池相接触的机会. 当液流束与熔池接触时, 电弧空间发生短路, 于是电弧熄灭(图 6c, d). 随后液流束发生破断, 而电弧重新引燃(图 6e). 显然, 与传统的短路过渡 MAG 焊的不同之处在于, 高速旋转短路过渡 MAG 焊的电弧、液锥和液流束都

始终处于高速旋转状态，熔滴过渡频率较高（约为750 Hz），同时伴随着较大的焊接飞溅.

由于焊丝端部的液态金属绕焊丝轴线高速旋转，使得液锥末端的液流束受到较大的旋转离心力的作用，再加上液流束与熔池短路时，短路电流急剧增大（这一点与传统的短路过渡类似），它所引起的电磁收缩力强烈地压缩液流束，从而加快液流束脱离液锥，因此旋转短路过渡的频率很高.但是由于高速旋转的液流束甚至是液锥不断地冲击熔池[3]，容易引起熔池内部液态金属的离心喷溅，形成了较大的飞溅.

而98%Ar+2%$O_2$ 气体保护的旋转短路过渡MAG 焊接过程则如图7 所示. 试验参数为 $v_f$=20 m/min，$U_a$=33 V，$L_e$=25 mm，保护气体流量为20 L/min，其它参数同2.1 节.

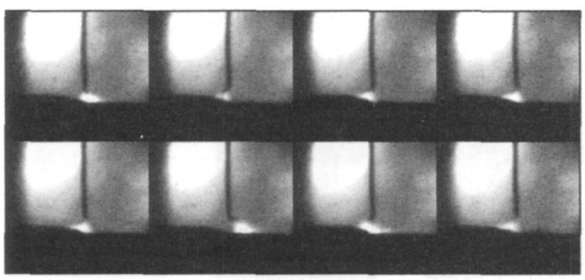

图7 98%Ar+2%$O_2$ 气体保护的高速旋转短路过渡 MAG 焊

Fig. 7 Shorting transfer process of high current density MAG welding with 98%Ar+2%$O_2$

由图7 可见，98%Ar+2%$O_2$ 气体保护的高速旋转短路过渡 MAG 焊与 80%Ar+20%$CO_2$ 气体保护的相似，当液流束与熔池短路时，由于高速旋转的液流束冲击熔池，导致熔池内部液态金属的离心喷溅，形成较大的飞溅. 但是与后者不同之处在于，前者的液流束与熔池短路时，电弧并没有熄灭，这说明前者的焊接电流通过焊丝端部的液态金属的分量较小[2]，而后者相对较大[2].

## 3 结 论

（1）随着焊丝伸出长度的增加，细丝大电流MAG 焊的第二临界电流值下降；当焊丝伸出长度相同时，保护气体为98%Ar+2%$O_2$ 的第二临界电流值要比保护气体为80%Ar+20%$CO_2$ 的大一些.

（2）细丝大电流 MAG 焊的熔滴过渡方式主要分为离心破断过渡、混合过渡（离心破断过渡与电爆炸过渡相结合）和旋转短路过渡.

（3）对于98%Ar+2%$O_2$ 气体保护的细丝大电流MAG 焊而言，电弧烁亮区均匀包覆了大部分液锥和全部的液流束，并且液流束在旋转离心力的作用能够顺畅地脱离液锥的束缚，焊接过程稳定，基本无飞溅.

（4）当电弧电压过低或者送丝速度过快，易形成旋转短路过渡 MAG 焊，此时由于高速旋转的液流束甚至是液锥不断地冲击熔池，造成了熔池内部液态金属的离心喷溅.

参考文献：

[1] Yin Shuyan, Chen Shujun, Wang Jun, *et al*. Mathematical model and magnetic-control mechanism of the stability of rotating spray transfer [J]. China Welding, 2003, 12(1): 57－61.

[2] 华爱兵. 磁旋弧MAG 焊接机理及应用研究[D]. 北京：北京工业大学, 2008.

[3] Lahnsteiner R. The T. I. M. E. process-an innovative MAG welding process[J]. Welding Review International. 1992, 11(1): 17－20.

[4] Lahnsteiner R. T. I. M. E. process produces fracture-proof welds[J]. Welding Design and Fabrication, 2002, 75(5): 32－35.

[5] Szubryt V, Marian K. Influence of welding parameters of butt joints made by various processes on their fatigue strength-FEM analysis[J]. Welding Research Abroad, 2004, 50(2): 35－41.

[6] Kammerhuber Ch, Sommerfeld R. High deposition MAG welding: used for welding bridges and structures[J]. Welding in the World, 1996, 38(3): 337－343.

作者简介：华爱兵，男，1977 年出生，博士研究生. 主要研究方向为焊接过程自动控制、新型逆变焊接电源和高效焊接工艺. 发表论文8篇.

Email：huaaibing@2008.sina.com

**A high-efficiency welding simulation method based on welding temperature** YAN Dongyang[1], SHI Qingyu[1], WU Aiping[1], Silvanus JUERGEN[2] (1. Department of Mechanical Engineering, Tsinghua University, Beijing 100084, China; 2. European Aeronautic Defence and Space Company Innovation Works, Munich 8166, Germany). p 77—80

**Abstract**: A lot of computed methods which improve the efficiency of welding simulation were discussed, and base on line-gauss heat source model, a new method was presented which was called temperature function method. Compared with line-gauss heat source model, the control variable in temperature function method was changed from heat input to welding temperature, which led to more consistent between welding temperature field from simulation and experiment in width and thickness direction of model. This new high-efficiency simulation method was validated by a model of friction stir welding on Al alloy sheet in this paper. The simulation results show that not only the residual stress and distortion of the sheet from temperature function method is similar with that from moving heat source model method, which is validated by the experimental results, but also the efficiency of new method is significant increased, and achieves the time request of welding simulation in engineering application.

**Key words**: welding; numerical simulation; high-efficiency simulation; line-gauss heat source

**Effects of interval of enhancive voltage on micro-arc oxidation coatings of magnesium alloy AZ91D** LÜ Weiling[1], MA Ying[1], CHEN Tijun[1], CHEN Ming[1], YANG Jian[2], HAO Yuan[2] (1. State Key Laboratory of Gansu Advanced Non-ferrous Metal Materials, Lanzhou University of Technology, Lanzhou 730050, China; 2. Key Laboratory of Non-ferrous Metal Alloys and Processing, Ministry of Education, Lanzhou University of Technology, Lanzhou 730050, China). p 81—84

**Abstract**: The effects of interval of enhancive voltage on micro-arc oxidation (MAO) coating of magnesium alloy AZ91D were investigated in silicate electrolyte. The microstructures were studied with TT230 digital coating thickness gauge, JSM-6700F scanning electron microscope, 2206 surface roughness measuring instrument and W-92 Coating adhesion scratch test machine, and the corrosion and wear resistance were assessed by means of CHI660C electrochemistry workstation and UMT-2MT ball-block reciprocating friction tester. The results show that with the increasing of interval of enhancive voltage, all of the thickness, roughness and bonding force of MAO coating always increase. The porosity of the coatings first increases, then decreases; it is up to its maximum values when interval of enhancive voltage is 150 s. The MAO coatings have the better corrosion and wear resistance than matrix metal, which have the best corrosion resistance as interval of enhancive voltage is 150 s and the best wear resistance as enhancive voltage is 60 s.

**Key words**: magnesium alloy AZ91D; micro-arc oxidation; enhancive voltage interval; corrosion resistance; wear resistance.

**All position pipe welding device for remote welding** DONG Na[1], GAO Hongming[1], ZHANG Yonghe[2], LI Haichao[1], WU Lin[1] (1. State Key Laboratory of Advanced Welding Production Technology, Harbin Institute of Technology, Harbin 150001, China; 2. Lanzhou Institute of Physics, Lanzhou 730000, China). p 85—88

**Abstract**: An all-position automatic minor-caliber pipe welding device used in a remote welding robot was designed for solving the problem of pipe maintenance in nuclear environment. The design analysis, working principle and automatic control parts of the device are described. The verification experiment about the device function was carried out by using the remote welding robot with the vision and force sensor. Results show that the device adapts the automatic assembling and disassembling requirement and has accurate position control. The circular motion error satisfies the demand of the all position welding. The actual welding results are good and prove that the device can be used in remote welding.

**Key words**: remote welding; terminal environment; pipe maintenance; all position welding

**Effect of carbon on impact toughness of metal deposited with high strength austenite electrodes** XUE Gang[1], ZHAO Fuchen[1], JING Yanhong[2], NIU Jicheng[1], ZHANG Yonghui[1], GAI Dengyu[3] (1. Luoyang Ship Material Research Institute, Luoyang 471039, China; 2. Henan Diesel Engine Industry CO., Ltd, Luoyang 471039, China; 3. College of Material Science & Chemical Engineering, Harbin Engineering University, Harbin 150001, China). p 89—92

**Abstract**: The impact toughness of metal deposited by high strength austenite electrodes with different carbon content was tested. The microstructure of the impact fractures and the eroded samples were analyzed by SEM. The second-phase was analyzed with the energy spectrometer and the TEM. The solidifying phases and the content of second-phase were calculated with the thermodynamic simulation software. The results indicate that the impact toughness reduces with the carbon increasing. The main cause is that the increasing of carbon content induces the shape changing from particles to slices, the dimension and the content increasing of the carbides forming in the solidification. The carbides weaken the continuity of the austenite base. And the brittle carbides crash easily in the crack spreading. These reduce the impact toughness of the deposited metal.

**Key words**: carbon; austenite; carbide; impact toughness

**Mechanics of drop transfer for high-current density MAG welding process** HUA Aibing[1], YIN Shuyan[2], CHEN Shujun[2], BAI Shaojun[2], ZHANG Xiaoliang[2] (1. Wise Welding Technology & Equipment Limited Company, Beijing 100076, China; 2. College of Mechanical Engineering and Applied Electronics Technology, Beijing University of Technology, Beijing 100022, China). p 93—96

**Abstract**: With the help of high-speed camera, the fundamental character of high current density MAG welding process with

two types of conventional shielded gas is analyzed. The influence of wire extension and shielded gas component on the second critical current is researched. So the mechanics of drop transfer of high-current density MAG welding process is disclosed, which is centrifugally breaking transfer, mixed transfer and rotating short transfer. Moreover, the reason of why high-current density MAG welding process with the shielded gas of 80% Ar and 20% $CO_2$ cannot be used is found. The application practicability of high effective welding for high-current density MAG welding process with the shielded gas of 98% Ar and 2% $O_2$ is built.

**Key words**: high current density MAG welding; the second critical current; centrifugally breaking transfer; rotating short transfer

**Prediction of residual stresses distribution in strength-mismatched butt joints using finite element method** ZHAO Zhili[1,2], YANG Jianguo[2], LIU Xuesong[2], FANG Hongyuan[2] (1. School of Materials Science and Engineering, Harbin University of Science and Technology, Harbin 150040, China; 2. State Key Laboratory of Advanced Welding Production Technology, Harbin Institute of Technology, Harbin 150001, China). p 97—100

**Abstract**: The influence of mis-match ratio and total width of cover pass on distributions of welding residual stresses are studied by finite element method for the application of undermatching butt joint of high strength steel. Although the weld strength mismatch effects are confined to a small region in the weld, all critical zone of fatigue failure such as weld toe and root of weld are located in this region. At weld toe, the magnitude of the longitudinal residual stresses increases and the magnitude of transverse residual stress decreases with increasing mis-match ratio. The magnitudes of the longitudinal residual stresses and transverse residual stress increase less with the increasing of total width of cover pass, but the position of peak value changes. The peak value of transverse residual stress of generic undermatching butt joints is located at base metal, but that of equal load-carrying undermatching butt joint corresponding to the increasing of total width of cover pass is located at weld toe.

**Key words**: mis-match ratio; welding residual stress; butt-welded joint; weld toe

**Microstructure and formation characteristics of rotating arc horizontal GMAW joint** GUO Ning, LIN Sanbao, ZHANG Yaqi, YANG Chunli (State Key Laboratory of Advanced Welding Production Technique, Harbin Institute of Technology, Harbin 150001, China). p 101—104

**Abstract**: Rotating arc horizontal GMAW can solve the dripping of the molten pool in the horizontal welding. The rotating arc process not only can reduce the welding heat input by prolonging the welding path in the some welding distance caused by the arc rotation, but also disperse the arc force to affect the sidewall periodically resulting in supporting the fusion metal near the upper groove. The characteristics of joint formation in rotating arc horizontal GMAW was studied. The asymmetry of the microstructure in the joint due to the rotation of the arc was discovered. The reason and the mechanism of this phenomenon was analyzed and interpreted.

**Key words**: horizontal welding; joint characteristics; rotating arc

**Vision system of butt joint gap width measurement for laser welding** WU Jiayong, WANG Pingjiang, CHEN Jihong, CHEN Zhiyi (National NC System Engineering Research Center, Huazhong University of Science and Technology, Wuhan 430074, China). p 105—108

**Abstract**: Laser welding process has demanding requirements on quality of butt joint preparation, especially on joint gap width and mismatch, the butt joint gap being narrow and little mismatch. Due to the inadequate lateral resolution or measuring principle limitation, current vision sensors can not measure the gap width accurately. In this paper, a vision system of joint gap width measurement is designed using the CCD camera with telecentric lens and diode laser, and a joint gap detection algorithm is proposed based on gray projecting integral approach. The experimental results demonstrate that the gap width measurement system can extract the joint border and joint gap width accurately; joint gap detection algorithm has self-verification ability to a certain extent. Accuracy of the measurement is better than 0.015 mm for a butt joint specimen with 0.05 mm gap width.

**Key words**: butt joint; gap width; laser welding; vision measurement

**Experimental investigation of friction stir welding of 7050 aluminum** WANG Ting[1], ZHU Danyang[2], LIU Huijie[1], FENG Jicai[1] (1. State Key Laboratory of Advanced Welding Production Technology, Harbin Institute of Technology, Harbin 150001, China; 2. Department of Material Science, Harbin Institute of Technology, Harbin 150001, China). p 109—112

**Abstract**: 7050-T7451 aluminum alloy was welded in friction stir welding at different welding parameters. The structure of the joints was studied with optical microscopy and TEM. Tensile strength and hardness distribution of the joints were tested. The mechanical properties, the microstructure and welding defects of the joints were controlled by changing welding parameters. The tensile strength of the joint was up to 88% of that of base metal at the parameters with tool traverse speed of 200 mm/min and rotation rate of 800 r/min. The fracture location was in HAZ in the joints welded in higher heat input; when the heat input was lower, kissing bond was produced in the root of the joint, and then fracture initiated from the location of the defect stretched. The result showed that dynamic recrystallization occurred in nugget zone together with the precipitates dissolved. Precipitates were coarsened in HAZ accompanying with the presence of precipitate-free zone.

**Key words**: friction stir welding; aluminum alloy; microstructure; mechanical property; fracture characterization